RARE METALS

ORIGINAL ARTICLE

Microstructure and texture evolution of TB8 titanium alloys during hot compression

Qiu-Yue Yang, Min Ma, Yuan-Biao Tan* , **Song Xiang, Fei Zhao, Yi-Long Liang**

Abstract In this study, microstructure and texture evolution of TB8 titanium alloys during hot deformation were investigated by using electron back-scattered diffraction (EBSD) analysis. The results showed that dynamic recrystallization (DRX) behavior of TB8 titanium alloys was drastically sensitive to the strain. As the true strain raised from 0.2 to 0.8, the degree of DRX gradually increased. The nucleation mechanism of recrystallization was observed, including discontinuous dynamic recrystallization (DDRX) resulting from the bulging of original boundaries. Furthermore, continuous dynamic recrystallization (CDRX) occurred because of the transformation of low-angle grain boundaries (LAGBs) to high-angle grain boundaries (HAGBs) in the interior of the original deformed grains. The texture evolution of TB8 titanium alloy during hot deformation process was analyzed in detail, and five texture components were observed, including $\{001\}\langle100\rangle$, $\{011\}\langle100\rangle$, $\{112\}\langle110\rangle$, $\{111\}\langle110\rangle$, and $\{111\}\langle112\rangle$. As the true strain increased, deformation textures were gradually weakened due to an increase in the volume fraction of DRX grains. When the true strain was 0.8, the main texture components consisted of the recrystallization texture components of the $\{001\}\langle100\rangle$ and $\{011\}\langle100\rangle$ textures.

Keywords TB8 titanium alloys; Hot compression; Microstructure; Texture evolution

Q.-Y. Yang, Y.-B. Tan*, S. Xiang, F. Zhao, Y.-L. Liang
College of Materials and Metallurgy, Guizhou University, Guiyang 550025, China
e-mail: ybtan1@gzu.edu.cn

M. Ma
College of Materials Science and Engineering, Hunan University of Science and Technology, Xiangtan 411201, China

1 Introduction

TB8 titanium alloy has been widely used to produce aircraft fasteners of gas turbine aero-engine due to its ultrahigh strength, exceptional ductility, and excellent corrosion resistance after solution and aging treatment [1, 2]. However, a larger deformation resistance is produced during thermo-mechanical processing of the TB8 titanium alloy, which strongly affects the hot workability of the alloy. Moreover, the mechanical properties of TB8 titanium alloy are significantly dependent on the microstructure and texture obtained during the manufacturing process. Therefore, controlling the microstructure and texture is of great significance to achieve superior mechanical properties in TB8 titanium alloy. Generally, the deformation mechanisms including adiabatic shear, flow localization, dynamic recovery (DRV), and dynamic recrystallization (DRX) could occur for metal materials during thermo-mechanical processing. DRV and DRX were widely considered as an effective method to refine grains and obtain better formability of alloys during industrial production, which is associated with processing variables, for instance, strain rate, deformation temperature, and strain. Thus, in order to improve the hot workability and mechanical properties of metal materials, it is quite significant to make a deep understanding on the relationship between processing parameters and the microstructure as well as texture evolution of metal materials during hot deformation.

Recently, a considerable number of researches have been launched to study the microstructure and texture evolution of titanium alloys and other alloys during thermo-mechanical processing [3–11]. Wu et al. [3] reported that two various nucleation mechanisms related to DRX, including continuous dynamic recrystallization (CDRX) and discontinuous dynamic recrystallization

(DDRX), were observed in the Ti–22Al–25Nb alloy. At a strain of 0.36, the main texture components of the β phase were {110}⟨110⟩, {110}⟨112⟩, and {112}⟨110⟩ in the deformed Ti–22Al–25Nb alloy. As the strain increased, the texture components of {110}⟨110⟩ and {110}⟨112⟩ gradually decreased. Only the weak texture components of {111}⟨112⟩ and {001}⟨110⟩ were observed at a strain of 1.2. The deformation textures were obviously weakened due to the formation of random orientations in the DRX grains. Chen et al. [4] revealed the microstructure and texture evolution of Ti-7333 alloys during continuous cooling hot deformation. The results showed that the main texture components of the β phase were {110}⟨111⟩ and {115}⟨552⟩ at a strain of 0.1, while the components were {100}⟨110⟩ and {001}⟨100⟩ at a strain of 0.91 after hot deformation. The texture component of {001}⟨100⟩ was the dominant deformation texture for the Ti-7333 alloys during continuous cooling hot deformation. Ghasemi et al. [5] investigated the dynamic recrystallization behavior of BT9 titanium alloy. The results showed that the nucleation mechanism of DRX in BT9 titanium alloy was CDRX. Wang et al. [6] found that the nucleation mechanism of DRX was DDRX at the initial stage of plastic deformation, while it was CDRX at the late stage of plastic deformation. In summary, the microstructure and texture evolution in different titanium alloys are obviously different because of the difference in alloy compositions.

Some investigations on hot deformation behavior of TB8 titanium alloys have also been widely reported [12–14]. Duan et al. [12] and Tang et al. [13] analyzed the hot deformation behavior of TB8 titanium alloys that deformed in α + β and single β regions and established an accurate constitutive models to characterize the relationship between flow stress (σ), deformation temperature (T), and strain rate (ε̇). In our previous work, the effect of initial grains on the flow behavior of TB8 titanium alloy was investigated and the optimum processing parameter was 900 °C/1 × 10^{-3} s^{-1} for the alloys solution-treated at 900 °C for 30 min. Thermomechanical processing is quite complex, and detailed investigation is needed to further study the microstructure and texture evolution of TB8 titanium alloys under different deformation conditions. However, there have been few studies about the microstructure and texture evolution of TB8 titanium alloys during the hot compression test. Thus, the objective of the present investigation is to thoroughly reveal the microstructure and texture evolution of TB8 titanium alloys with true strain.

2 Experimental

A forged bar of TB8 titanium alloy with a diameter of 60 mm was used in this study. The transition temperature

of the β phase ($T_β$) of this alloy was tested to be 815 °C [12]. The microstructure of the alloy consists of a single β phase above the $T_β$ temperature, while it is composed of α + β phase below the $T_β$ temperature. The melting point of the alloy is (1740 ± 40) °C, and the temperature of static recrystallization is ∼ 696 °C, according to the empirical equation of $T_R = 0.4T_m$ (T_R is the temperature of static recrystallization, and T_m is the melting point of the alloy). To reveal the microstructure and texture evolution of this alloy during the hot compression test, the forged bar was heated at 900 °C for 30 min in a high vacuum environment and subsequently cooled in water. As shown in Fig. 1a, the initial microstructure of the solution-treated samples was composed of a uniform and equiaxed recrystallized grain structure with a grain size of ∼ 87 μm. It is expected from Fig. 1b that the microstructure of the solution-treated samples consisted of a single β phase structure.

Cylindrical samples of 12 mm in height and 8 mm in diameter were obtained from the heat-treated bars. Hot compression testing of the samples was conducted on a Gleeble 3500 testing system. All deformed samples were directly heated to the deformation temperature with a rate of 20 °C·s^{-1} and soaked for 5 min to eliminate the temperature gradient existed in the deformed samples before deformation. The deformation temperature is 900 °C, and the strain rate is 1 × 10^{-3} s^{-1}. The deformed samples were compressed to a true strain of 0.2, 0.4, 0.6, and 0.8, respectively, and subsequently water-quenched to retain the deformed microstructures formed under the high-temperature condition. A schematic of the applied hot deformation is shown in Fig. 2. To study the microstructure and texture evolution of TB8 titanium alloys during hot compression testing, the deformed samples were machined along their radial direction. The microstructure and texture evolution of the deformed samples were analyzed by using the electron back-scattered diffraction (EBSD) technique. Samples were prepared for EBSD through grinding and electro-polishing in a solution of 70 vol% CH$_3$OH, 10 vol% HClO$_4$, and 20 vol% (CH$_2$OH)$_2$ at the voltage of 18 V for 15 s. A Hitachi S-3400N-II scanning electron microscope with an EBSD system operating at 20 keV was used. The step size for EBSD orientation observation was 0.8 μm.
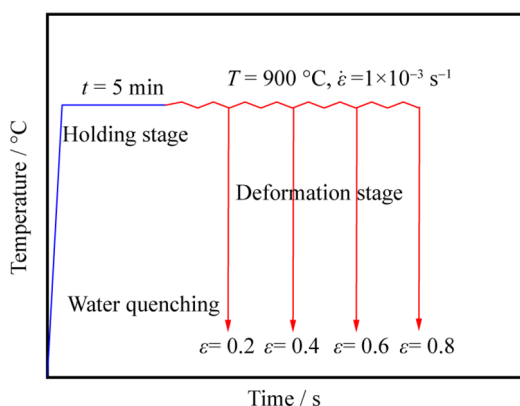
3 Results and discussion

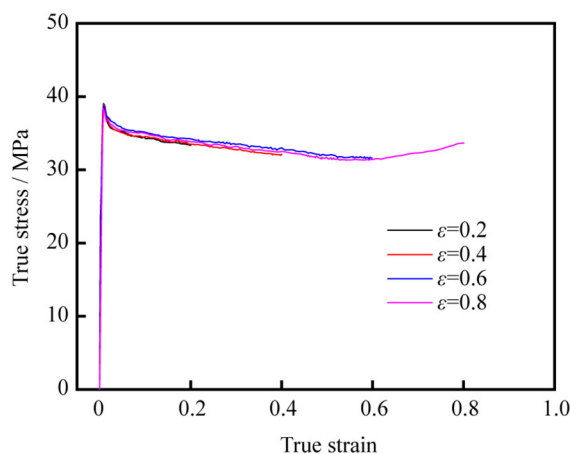### 3.1 Microstructural evolution of deformed samples during hot deformation

Figure 3 displays the flow curves of TB8 titanium at different strains, which exhibits a typical dynamic
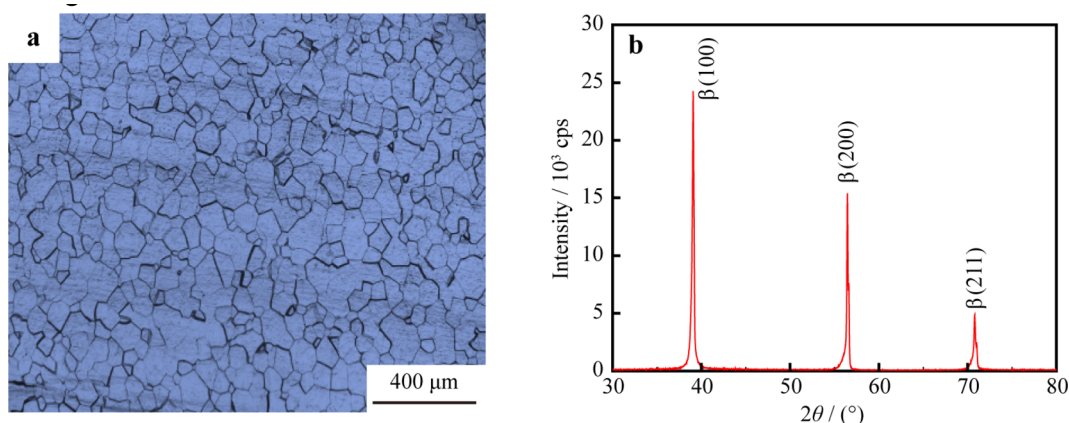
Fig. 1 a Microstructure and **b** XRD pattern of TB8 titanium alloy after solution treatment at 900 °C for 30 min

Fig. 2 Schematic diagram of hot deformation tests

Fig. 3 True stress–strain curves of TB8 titanium alloy under different deformation conditions

recrystallization characteristic. The flow stress rapidly attained a peak at the initial stage of hot deformation, which was attributed to generation and multiplication of dislocations. Subsequently, the flow stress decreased to a stable value due to the occurrence of DRX.

Figure 4 illustrates the optical microstructures of the solution-treated samples, which were deformed at different true strains. Obviously, the strain strongly affected the microstructure evolution of the TB8 titanium alloys during hot deformation. As shown in Fig. 4a, the initial equiaxed grains were elongated along the direction perpendicular to the compression axis and some serrated grain boundaries were observed at a true strain of 0.2. Generally, a high strain gradient could be formed on both sides of the serrated grain boundaries, which is considered as a prior site for the nucleation of DRX grains [15]. In addition, a few fine newly recrystallized grains formed in the local region of the original grain boundaries. This suggests that the nucleus of DRX grains preferentially forms on the prior grain boundaries at a true strain of 0.2. When true strain reached 0.4, a significant amount of new recrystallized grains was observed and the microstructures of the deformed samples presented a typical necklace structure, as

shown in Fig. 4b. With an increase in the strain, DRX occurred in most of the deformed grains and the volume fraction of recrystallized grains obviously increased, as shown in Fig. 4c. As the true strain increased to 0.8, the microstructures of the deformed samples consisted of numerous fine equiaxed recrystallized grains (Fig. 4d). It is apparent that increasing strain significantly promoted the occurrence of DRX during thermo-mechanical processing. This is ascribed to an increase in deformation storage energy (DSE) with increasing strain. A high DSE accelerates the movements of dislocation and the migration of grain boundaries during thermo-mechanical processing, which provides a strong driven force for the nucleation and growth of DRX grains.

3.2 Dynamic recrystallization mechanism in TB8 titanium alloys during hot deformation

In general, the dynamic recrystallization mechanism of metallic materials mainly includes geometric dynamic
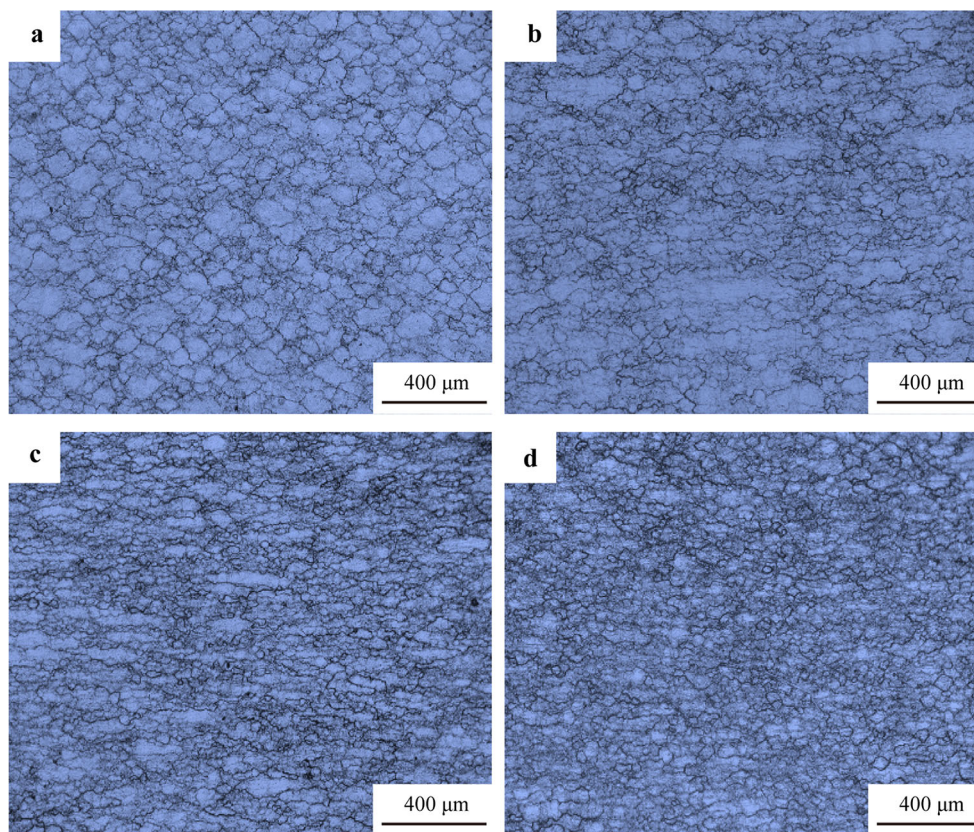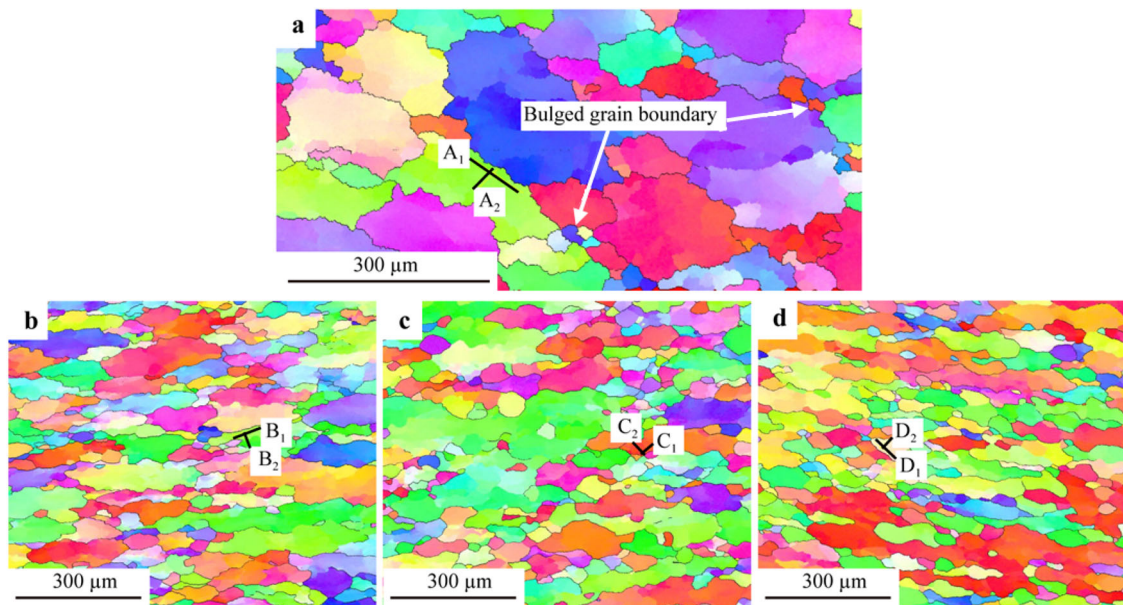
Fig. 4 OM images of solution-treated samples deformed at different true strains of **a** 0.2, **b** 0.4, **c** 0.6, and **d** 0.8

recrystallization (GDRX), DDRX, and CDRX during hot deformation. The GDRX mechanism only occurs under heavy deformation where the original deformed grains would split into fine new recrystallized grains. In the current investigation, the true strain was less than 0.8; therefore, the GDRX mechanism could not occur during hot compression of the TB8 titanium alloy. In the DDRX mechanism, the nucleation of recrystallized grains is initiated at the grain boundaries of original deformed grains and forms via bulging of the original boundaries, subsequently growing towards the interior of the initially deformed grains. For the CDRX mechanism, as the strain increases during hot deformation, the microstructure presents a continuous change from the generation of dislocations and the formation of subgrains via annihilation and rearrangement of the dislocation to the form of new recrystallized grains by the progressive rotation of subgrains in which LAGBs gradually transformed to HAGBs. Typically, the evolution of subgrains can be depicted by the variation in the cumulative misorientation (point to origin) and local misorientation (point to point) [15, 16].

To further reveal the nucleation mechanism of DRX in TB8 titanium alloys during hot compression, EBSD analysis was used for the solution-treated samples deformed at various true strains, as illustrated in Fig. 5. Noticeably, the

strain presents a pronounced influence on the microstructure evolution of the TB8 titanium alloys.

Figure 6 exhibits the variation of the cumulative and local misorientation along the lines marked in Fig. 5. It could be observed from Fig. 6a, b that the values of local misorientation along line A_1 were less than 5°, while the values of local misorientation along line A_2 were less than 3° at a true strain of 0.2. At the same time, the values of cumulative misorientation along lines A_1 and A_2 were less than 10°. This indicates that LAGBs mainly accumulated near initial grain boundaries and the subgrain rotation was not distinct under relatively low strains. It is shown from Fig. 5a that a few fine new recrystallized grains formed in the grain boundaries of the original deformed grains by the bulging of the original boundaries, which were marked with arrows. This suggests that the nucleation mechanism of DRX is mainly the DDRX mechanism at a true strain of 0.2. When the true strain increased to 0.4, the values of cumulative misorientation and local misorientation along line B_1 were less than 10°. However, the values of cumulative misorientation along line B_2 easily exceed 12° at a distance of $\sim$ 33 μm (Fig. 6c, d). It is implied that the misorientation accumulates and the progressive subgrain rotation has been developed in the grain interior, which would accelerate the development of CDRX. It was

Fig. 5 Inverse pole figures (IPFs) of solution-treated samples deformed at different true strains of **a** 0.2, **b** 0.4, **c** 0.6, and **d** 0.8
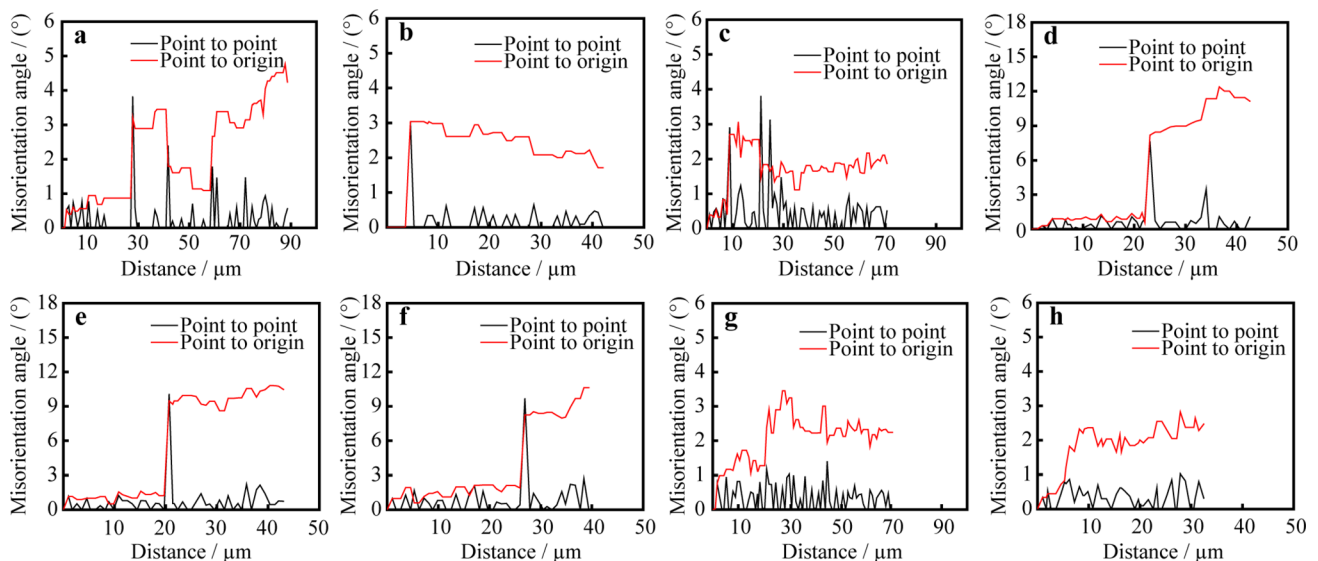
Fig. 6 Variation of misorientation angles along lines marked in Fig. 5: **a** A_1, **b** A_2, **c** B_1, **d** B_2, **e** C_1, **f** C_2, **g** D_1, and **h** D_2

interesting to note that a pronounced gap was observed at a distance range of 22–23 μm. This can be ascribed to the deformation bands with different orientations resulting from different slip systems in the adjacent grains [3, 15, 16]. As the true strain reached 0.6, the misorientation angle gradient along lines C_1 and C_2 raised obviously, as shown in Fig. 6e, f. Both cumulative misorientations along lines C_1 and C_2 exceed 10° at a distance of ∼ 35 and 38 μm, respectively. This implies that the subgrain rotation was further developed and the developing of DRX induced by subgrain rotation was more distinct with increasing the true strain. These results show that the CDRX mechanism was the primary nucleation mechanism of DRX when the

true strain was higher than 0.4. When the true strain further increased to 0.8, it can be observed from Fig. 6g, h that the values of cumulative misorientation predominantly reduced and were less than 4°, revealing that the DRX grains with low dislocation density have superseded the deformed grains.

Figure 7 exhibits the distribution histograms of grain boundary misorientation angles from 2° to 65° for the solution-treated samples deformed at various true strains. Figure 8 shows the variation in the number fraction of HAGBs and LAGBs with true strain. Here, HAGBs are defined as the grain boundaries with a misorientation angle beyond 15° and LAGBs are defined as the grain boundaries

with a misorientation angle between 2° and 15°. As illustrated in Fig. 7a, the grain boundaries were mainly HAGBs and the average misorientation angle was calculated to be ~ 23.11° at the true strain of 0.2. It can be observed from Fig. 8 that the number fraction of LAGBs was 47.9%, while the number fraction of HAGBs was 52.1%. This is associated with a small strain, only leading to the generation of a small number of dislocations. The prior grain boundaries remained as dominant grain boundaries at the original deformation stage. When the true strain was 0.4, the number fraction of LAGBs rose to 63.2% and the average misorientation angle was ~ 16.54°, which was less than that observed at a true strain of 0.2 (Figs. 7b, 8). This indicates that rapid generation of mobile dislocations occurs during plastic deformation. Meanwhile, the deformation storage energy remains relatively low under this strain condition, which is insufficient for the nucleation of most DRX grains. Thus, the number fraction of LAGBs is high. As the true strain increased from 0.4 to 0.8, the number fraction of LAGBs decreased from 63.2% to 55.2% (Fig. 8), while the average misorientation angle gradually increased from 16.54° to 18.39° (Fig. 7b–d). This is attributed to an increase in the degree of dynamic

recrystallization and a decrease in the number of dislocation substructures. It is commonly known that plastic deformation is caused by the movement of mobile dislocations from one grain to adjacent grains [15, 17]. When the strain exceeds a critical value, mobile dislocation can rapidly generate during plastic deformation, giving rise to the formation of a high dislocation density network. With the increase in true strain, subgrains will form through annihilation and rearrangement of dislocation substructures and then transform into the DRX grains through combination and rotation of the subgrains [18]. When the strain was further increased, the volume fraction of DRX grains with a low density of dislocation obviously increased, which distinctly decreased dislocation substructure. Therefore, the number fraction of LAGBs decreased with the increase in true strain, while the number fraction of HAGBs increased.

3.3 Texture evolution of TB8 titanium alloys during hot deformation

The mechanical properties of TB8 titanium alloys are significantly affected by the texture formed during thermo-
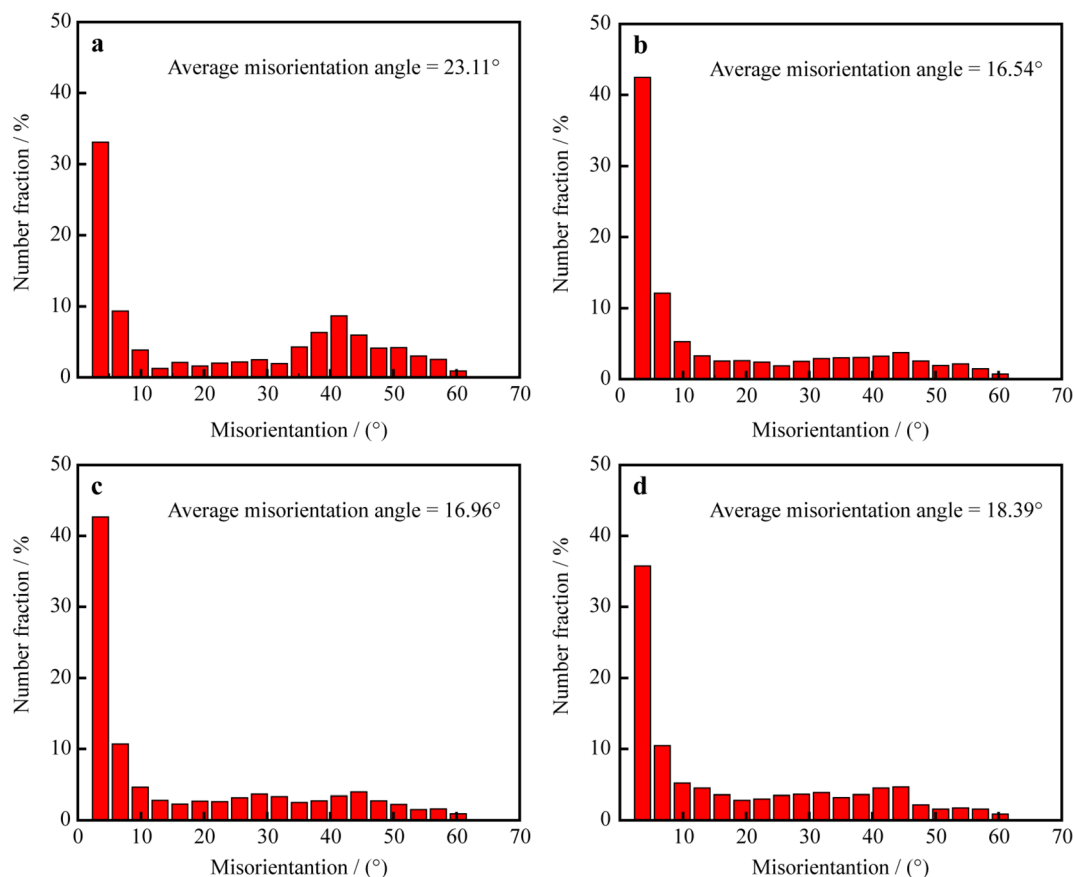

Fig. 7 Distribution histograms of misorientation angles in 2°–65° for solution-treated samples deformed at different true strains of **a** 0.2, **b** 0.4, **c** 0.6, and **d** 0.8

mechanical processing. Thus, it is rather necessary to reveal the texture evolution of TB8 titanium alloys during thermo-mechanical processing in detail. It is commonly known that the texture of the deformed materials can be characterized by using the orientation distribution function (ODF). In the ODF sections, each texture component is described by the Euler angles (φ_1, Φ, φ_2) and the intensity of texture is characterized by the colored contour. For body-centered cubic (bcc) metallic materials, the typical texture components can be presented in the ODF sections with a constant φ_2 of 45° [19–22].

Figure 9 illustrates ODF sections with a constant φ_2 of 45° for the solution-treated samples deformed at different true strains. A schematic drawing of the section ($\varphi_2 = 45°$) of ODF with typical texture components for bcc materials is exhibited in Fig. 9e. It can be observed from Fig. 9a that the texture components were mainly η-fiber components of $\{001\}\langle100\rangle$ and $\{011\}\langle100\rangle$, α-components of $\{112\}\langle110\rangle$, as well as γ-fiber components of $\{111\}\langle110\rangle$ and $\{111\}\langle112\rangle$. Wu et al. [3], Sander and Raabe [19] have also reported that the most relevant texture components in the compressive titanium alloys mainly included the η-fiber, α-fiber, and γ-fiber. The textures of $\{001\}\langle100\rangle$, $\{011\}\langle100\rangle$ and $\{111\}\langle112\rangle$ are typical recrystallization texture components for the bcc metals, while the textures of $\{112\}\langle110\rangle$ and $\{111\}\langle110\rangle$ are dominant deformation textures [4, 19–26]. In order to analyze the effect of true strain on texture evolution, the volume fractions of different texture components at various true strains were calculated, as indicated in Fig. 10. The volume fractions of $\{001\}\langle100\rangle$, $\{011\}\langle100\rangle$, $\{112\}\langle110\rangle$, $\{111\}\langle110\rangle$, and $\{111\}\langle112\rangle$ textures were 9.6%, 10.2%, 5.2%, 3.3%, and 8.1% at a true strain of 0.2, respectively. As true strain increases from 0.2 to 0.8, the volume fractions of $\{111\}\langle110\rangle$ and $\{112\}\langle110\rangle$ textures evidently decrease to 0.3% and 0.4%, respectively. This indicates that the deformation textures were gradually weakened with the increase in true strain. Similar results were also observed in Ti–35Nb–7Zr–5Ta and Ti–15Mo–3Al–2.7Nb–0.2Si alloys [19, 24]. The weakening of the deformation texture is attributed to an increase in the volume fraction of DRX grains with true strain increasing. This suggests that in addition to deformation, the evolution of texture is also dominated by the processes of recrystallization when true strain increases to a considerable extent.

It was noted that the volume fraction of $\{001\}\langle100\rangle$ texture significantly increased as true strain increased from 0.2 to 0.8, while the volume fraction of the $\{011\}\langle100\rangle$ texture initially presented a rising trend and then dropped. This phenomenon is associated with the nucleation sites for the recrystallized grains. It was found from Fig. 11 that the $\{001\}\langle100\rangle$ texture was mainly observed in the recrystallized grains nucleated by the bulging of original boundaries
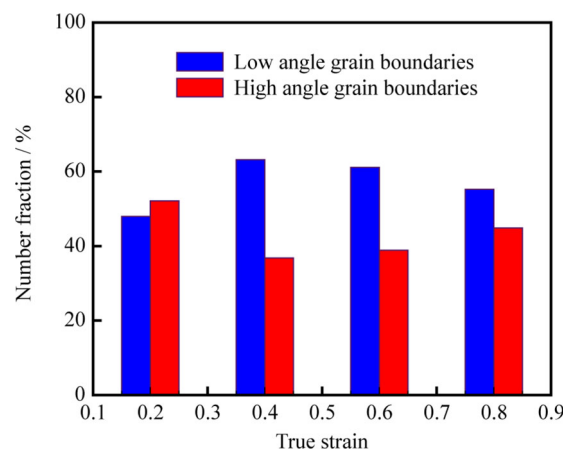
Fig. 8 Variation of number fraction of high-angle grain boundaries and low-angle grain boundaries with true strain

and a small quantity of the $\{001\}\langle100\rangle$ texture presented in the recrystallized grains nucleated within the deformed original grains and at the triple junctions of original grains. The grain boundary bulging nucleation, namely strain-induced boundary migration (SIBM), was considered to be an important nucleation mechanism of recrystallization for the deformed metals during hot deformation [27]. The nucleation of recrystallized grains formed at the grain boundaries with the SIBM due to the difference in the deformed stored energies and dislocation densities. It is widely known that recrystallized grains nucleated by the bulging of original boundaries can inherit the orientations from the adjacent matrices in the process of follow-up hot deformation, thus resulting in an increase in the texture intensity [28–30]. Moreover, the $\langle100\rangle$-oriented grains with a lower Taylor factor have a lower stored energy during hot deformation, which provides a driving force for the grain boundary migration from $\langle100\rangle$-oriented grains to other oriented grains, which means that the recrystallized grains with an $\langle100\rangle$ orientation nucleate and grow more easily compared with the recrystallized grains with other orientations during hot deformation; therefore, the volume fraction of $\{001\}\langle100\rangle$ texture increased with the increase in true strain. Li and Yang [29] also found that the $\{001\}\langle100\rangle$ texture was readily formed when the alloy underwent dynamic recrystallization during hot compression and a strong $\{001\}\langle100\rangle$ texture component was formed as deformation increased. For the $\{011\}\langle100\rangle$ texture, Barnett and Jonas [25] reported that the $\{011\}\langle100\rangle$ texture usually nucleated at shear band in the grains with $\{111\}\langle112\rangle$ orientation and the intensity of the $\{011\}\langle100\rangle$ texture gradually reduced with a drop in shear banding.

In the present investigation, flow localizations were readily produced in the center of the deformed samples along the radius direction during hot compressing of TB8
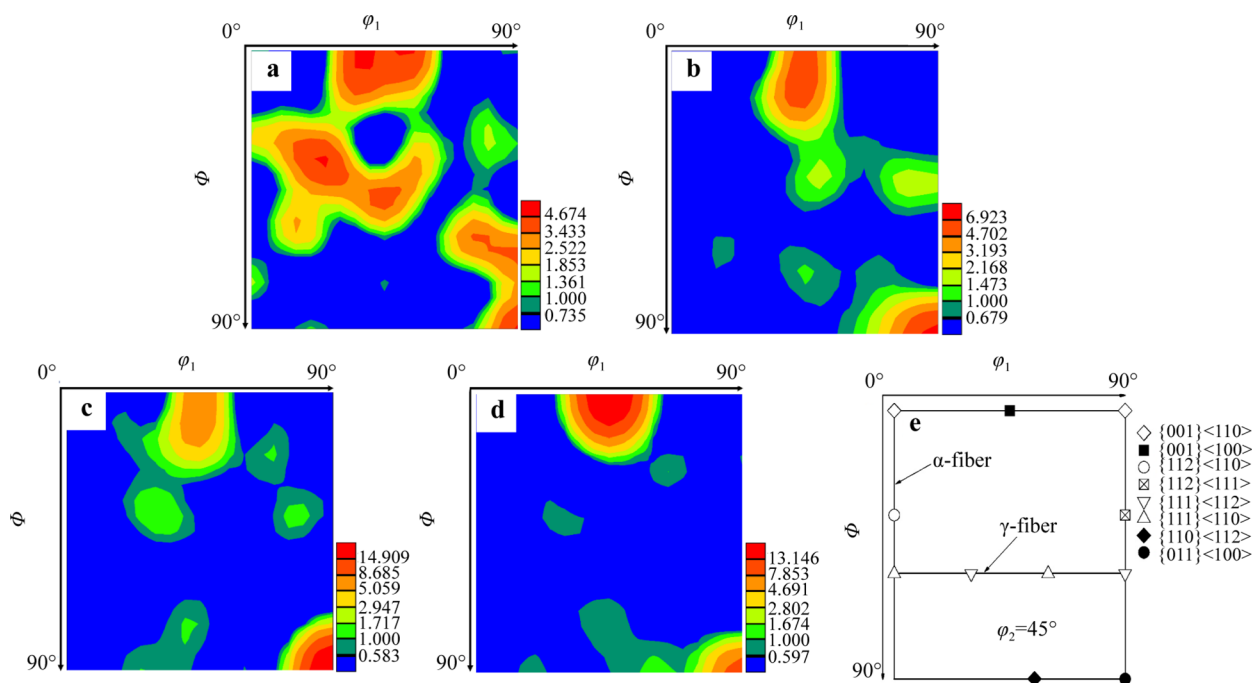
Fig. 9 Sections ($\varphi_2 = 45°$) of ODF for solution-treated samples deformed at different true strains of **a** 0.2, **b** 0.4, **c** 0.6, and **d** 0.8; **e** schematic drawing of section ($\varphi_2 = 45°$) of ODF with typical texture components for bcc materials
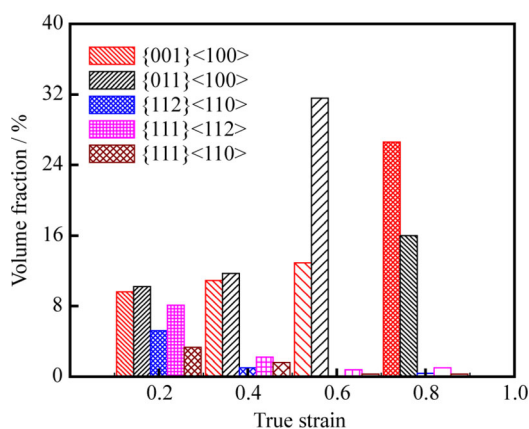
Fig. 10 Variation in volume fractions of different texture components with true strain for TB8 titanium alloys during hot deformation

titanium alloys due to the inhomogeneity of deformation, which promoted formation of the {011}⟨100⟩ texture. It was also observed from Fig. 11 that the majority of the {011}⟨100⟩ texture was primarily formed in the heavily deformed original grains, while a small amount of the {011}⟨100⟩ texture was produced in the recrystallized grains nucleated by the bulging of original boundaries. When the true strain was less than 0.6, both the volume fraction of recrystallized grains and the deformation degree of deformed original grains gradually increased with the increase in true strain, which caused an increase in the volume fraction of {011}⟨100⟩ texture. However, when the true strain increased to 0.8, a full recrystallization with

homogeneous microstructure was achieved and the deformed original grains disappeared, which gave rise to a decrease in the volume fraction of {011}⟨100⟩ texture.

It is also shown in Fig. 10 that the volume fraction of {111}⟨112⟩ texture gradually weakened with the increase in true strain. The {111}⟨112⟩ texture is commonly observed in bcc metals during warm and hot deformation [3, 4, 19, 25, 26]. Barnett and Jonas [25, 26] and Sander and Raabe [19] have reported that the {111}⟨112⟩ recrystallization texture mainly nucleated in shear bands and flow localizations, and the in-grain shear bands in {111}⟨112⟩ orientation could lead to lattice rotation to both Goss and near-normal direction (ND) fiber orientations with the increase in deformation. This shows that the volume fraction of the {111}⟨112⟩ texture would decrease with an increase in Goss nucleation and a decrease in the number of in-grain shear bands [25]. In the present work, the Goss {011}⟨100⟩ texture increased as true strain increased from 0.2 to 0.6, which gave rise to a decrease in the volume fraction of the {111}⟨112⟩ texture. Furthermore, a full dynamic recrystallization has taken place as the true strain reached 0.8, which may also lead to a decrease in the volume fraction of the {111}⟨112⟩ texture.

4 Conclusion

DRX behavior of TB8 titanium alloys is drastically sensitive to the strain. At a true strain of 0.2, some serrated grain
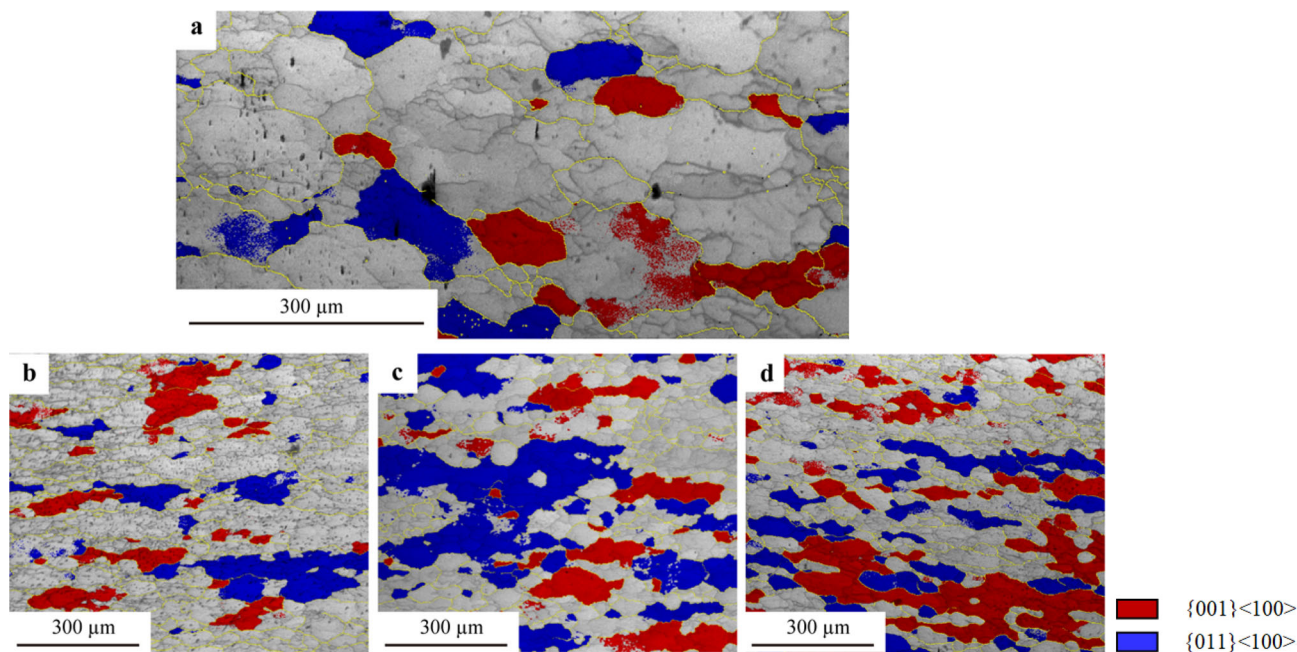
Fig. 11 EBSD analyses of nucleation sites for cube orientation {001}⟨100⟩ and Goss orientation {011}⟨100⟩ in TB8 alloys deformed at different true strains of **a** 0.2, **b** 0.4, **c** 0.6, and **d** 0.8

boundaries were observed and a few fine new recrystallized grains formed in the local region of original grain boundaries. With increasing true strain, the degree of DRX gradually increased. The CDRX and DDRX mechanisms are observed in the hot deformation process of TB8 titanium alloys. For the DDRX mechanism, the nucleation of new recrystallized grains forms in the grain boundaries of the original deformed grains via bulging of original boundaries. For the CDRX mechanism, the nucleation of new recrystallized grains is produced in the interior of the original deformed grains through the transformation of LAGBs to HAGBs. The texture evolution of TB8 titanium alloys in a hot deformation process is analyzed in detail. Five texture components are observed including the η-fiber components of {001}⟨100⟩ and {011}⟨100⟩, α-fiber components of {112}⟨110⟩, as well as γ-fiber components of {111}⟨110⟩ and {111}⟨112⟩. The volume fractions of {111}⟨110⟩, {112}⟨110⟩, and {111}⟨112⟩ textures evidently decrease as true strain increases from 0.2 to 0.8, while the volume fraction of {001}⟨100⟩ texture notably increases. The volume fraction of {011}⟨100⟩ texture initially increases as true strain increases from 0.2 to 0.8 and then subsequently decreases. When the true strain is 0.8, the main texture components consist of the {001}⟨100⟩ and {011}⟨100⟩ textures.

References

[1] Xu TW, Li JS, Zhang FS, Wang FY, Liu XH, Feng Y. Microstructure evolution during cold-deformation and aging response after annealing of TB8 titanium alloy. Rare Metal Mat Eng. 2016;45(3):0575.
[2] Tang B, Tang B, Han FB, Yang GJ, Li JS. Influence of strain rate on stress induced martensitic transformation in β solution treated TB8 alloy. J Alloys Compd. 2013;565:1.
[3] Wu Y, Kou HC, Wu ZH, Tang B, Li JS. Dynamic recrystallization and texture evolution of Ti–22Al–25Nb alloy during plane–strain compression. J Alloys Compd. 2018;749:844.
[4] Chen JH, Li JS, Tang B, Chen Y, Kou HC. Microstructure and texture evolution of a near β titanium alloy Ti–7333 during continuous cooling hot deformation. Prog Nat Sci Mater. 2019;29(1):50.
[5] Ghasemi E, Zarei-Hanzaki A, Farabi E, Tesař K, Jäger A, Rezaee M. Flow softening and dynamic recrystallization behavior of BT9 titanium alloy: a study using process map development. J Alloys Compd. 2017;695:1706.
[6] Wang G, Xu L, Tian YX, Zheng Z, Cui YY, Yang R. Flow behavior and microstructure evolution of a P/M TiAl alloy during high temperature deformation. Mater Sci Eng, A. 2011;528:6754.
[7] Zhang Y, Wang XP, Kong FT, Sun LL, Chen YY. Microstructure, texture and mechanical properties of Ti–43Al–9 V–0.2Y alloy hot-rolled at various temperatures. J Alloys Compd. 2019;777:795.
[8] Qu WT, Sun XG, Hui SX, Wang ZG, Yan L. High-temperature deformation behavior of a beta Ti–3.0Al–3.5Cr–2.0Fe–0.1B alloy. Rare Met. 2018;37(3):217.
[9] Mantri SA, Banerjee R. Microstructure and micro-texture evolution of additively manufactured β–Ti alloys. Addit Manuf. 2018;23:86.

Springer

[10] Yin LX, Liang SX, Zheng LY, Shi YD, Xie HL, Ma MZ, Liu RP. Microstructural and textural evolutions of TZ410 alloy under various rolling conditions. Mate. Charact. 2016;121:199.

[11] Lu SY, Ma FC, Liu P, Li W. Microstructure and mechanical properties of TiB reinforced titanium matrix composites with heat treatment. Chin J Rare Met. 2018;42(4):379.

[12] Duan YP, Ping L, Xue KM, Zhang Q, Wang XX. Flow behavior and microstructure evolution of TB8 alloy during hot deformation process. Trans Nonferrous Met Soc. 2007;17(6):1199.

[13] Tang B, Tang B, Han FB, Li JS, Yang GJ. Hot deformation behavior of TB8 alloy near the β–transus. Rare Metal Mat Eng. 2013;42(9):1761.

[14] Yang QY, Ma M, Tan YB, Xiang S, Zhao F, Liang YL. Initial β grain size effect on high-temperature flow behavior of TB8 titanium alloys in single β phase field. Metals. 2019;9(8):891.

[15] Lin YC, Wu XY, Chen XM, Chen J, Wen DX, Zhang JL, Li LT. EBSD study of a hot deformed nickel-based superalloy. J Alloys Compd. 2015;640:101.

[16] Lin YC, He DG, Chen MS, Chen XY, Zhao CY, Ma X, Long ZL. EBSD analysis of evolution of dynamic recrystallization grains and δ phase in a nickel–based superalloy during hot compressive deformation. Mater Des. 2016;97:13.

[17] Lin YC, Chen XM. A critical review of experimental results and constitutive descriptions for metals and alloys in hot working. Mater Des. 2011;32:1733.

[18] Chen XM, Lin YC, Chen MS, Li HB, Wen DX, Zhang JL, He M. Microstructural evolution of a nickel–based superalloy during hot deformation. Mater Des. 2015;77:41.

[19] Sander B, Raabe D. Texture inhomogeneity in a Ti–Nb–based β–titanium alloy after warm rolling and recrystallization. Mater Sci Eng, A. 2008;479:236.

[20] Yuan C, Gao X, Li JH, Bao XQ. Secondary recrystallization of Goss texture in magnetostrictive Fe–Ga-based sheets. Rare Met. 2020;39(11):1288.

[21] Xu YF, Yi DQ, Liu HQ, Wu XY, Wang B, Yang FL. Effects of cold deformation on microstructure, texture evolution and mechanical properties of Ti–Nb–Ta–Zr–Fe alloy for biomedical applications. Mater Sci Eng, A. 2012;547:64.

[22] Gupta A, Khatirkar RK, Kumar A, Thool K, Bibhanshu N, Suwas S. Microstructure and texture development in Ti–15 V–3Cr–3Sn–3Al alloy–possible role of strain path. Mater Charact. 2019;156:109884.

[23] Hölscher M, Raabe D, Lücke K. Relationship between rolling textures and shear textures in f.c.c. and b.c.c. metals. Acta Metall Mater. 1994;42(3):879.

[24] Chen Y, Li JS, Tang B, Kou HC, Xue XY, Cui YW. Texture evolution and dynamic recrystallization in a beta titanium alloy during hot-rolling process. J Alloys Compd. 2015;618:146.

[25] Barnett MR, Jonas JJ. Influence of ferrite rolling temperature on grain size and texture in annealed low C and IF steels. ISIJ Int. 1997;37(7):706.

[26] Barnett MR. Role of in-grain shear bands in the nucleation of ⟨111⟩//ND recrystallization textures in warm rolled steel. ISIJ Int. 1998;38(1):78.

[27] Humphreys FJ, Hatherly M. Recrystallization and Related Annealing Phenomena. 2nd ed. Oxford: Elsevier; 2004. 251.

[28] Hasegawa M, Yamamoto M, Fukutomi H. Formation mechanism of texture during dynamic recrystallization in γ–TiAl, nickel and copper examined by microstructure observation and grain boundary analysis based on local orientation measurements. Acta Mater. 2003;51(13):3939.

[29] Li K, Yang P. The formation of strong 100 texture by dynamic strain-induced boundary migration in hot compressed Ti–5Al–5-Mo–5V–1Cr–1Fe alloy. Metals-Basel. 2017;7(10):412.

[30] Gu B, Chekhonin P, Schaarschuch R, Oertel CG, Xin SW, Ma CL, Zhou L, Gan WM, Skrotzki W. Microstructure, texture and hardness of a metastable β–titanium alloy after bar-rolling and annealing. J Alloys Compd. 2020;825:154082.